

# Combining absorbing and nonreflecting boundary conditions for elastic wave modeling

Zaiming Jiang\*, John C. Bancroft, and Laurence R. Lines, CREWES project, University of Calgary

## Summary

The absorbing boundary conditions and the nonreflecting boundary condition are two of the most popular solutions to the computational boundary condition problem. We report our implementations of these boundary conditions within our staggered-grid finite-difference applications and describe their features. Then we present a method combining the absorbing boundary conditions and the nonreflecting boundary condition.

## Introduction

Computational boundary condition problems have been a persistent topic in the field of wave phenomena modelling. Migration algorithms also have to deal with boundaries.

There are a lot of solutions to the boundary condition problems. The most cited method about boundary conditions is the “absorbing boundary conditions” proposed by Engquist and Majda (1977), and Clayton and Engquist (1977). Another popular method called “nonreflecting boundary condition” was presented by Cerjan, Kosloff, Kosloff, and Reshef in 1985. There are some other solutions as well, such as “transparent boundary” by Long and Liow (1990) and “perfectly matched layer” method by Collino and Tsogka (2001).

This abstract reviews the absorbing and nonreflecting boundary conditions first, and then presents the combined boundary conditions.

## Boundary conditions

The elastic modeling method we use is based on the Madariaga-Virieux staggered-grid scheme (Virieux, 1986).

To illustrate the boundary conditions, a subsurface model, which contains a point diffractor in a homogenous medium, is designed. Figure 1 shows the geometry and the P-wave velocities, although the real subsurface model parameters used by the modeling algorithm are densities and Lamé coefficients.



Figure 1: A scatter point in a homogenous medium. This shows the P-wave velocities.

A rigid boundary is an idealized immovable interface. The boundary conditions are the vertical and horizontal components of displacement are zero at the boundary. Figure 2-a shows a vertical component snapshot of a rigid bottom boundary reflection. An explosive source is at the top center, and the generated P-wave, S-wave, and head wave propagate downward. The P-wave hits the rigid bottom boundary and a strong PP reflection is formed (there is no PS reflection). The boundary reflection is much stronger than the reflections from the point diffractor.

## Combining boundary conditions

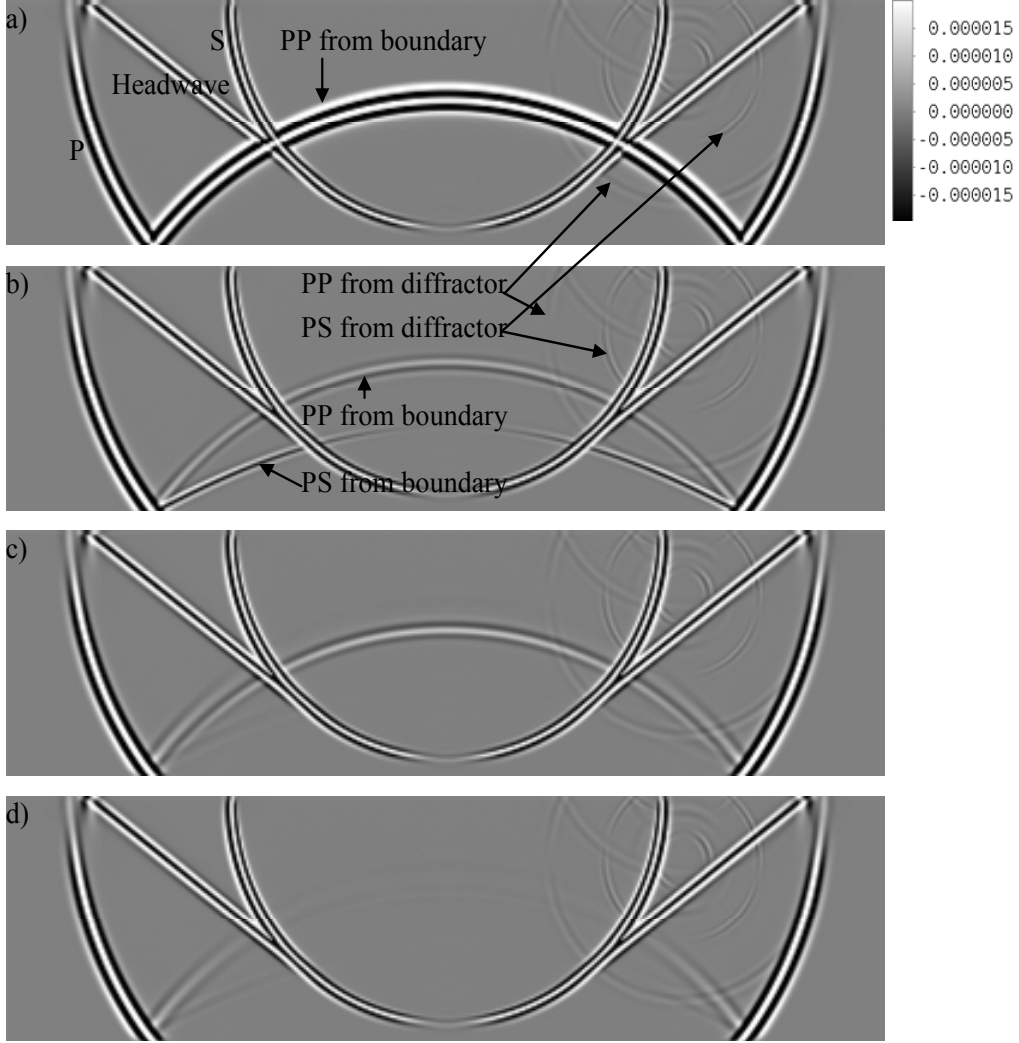


Figure 2: Bottom boundary reflection effects of different boundary conditions: a) rigid boundary condition, b) absorbing boundary conditions, c) non-reflecting boundary condition, and d) combined boundary conditions of absorbing and non-reflecting.

The absorbing boundary conditions A1 (Clayton and Engquist, 1977) for the bottom boundary of a 2D elastic subsurface model can be written as

$$\begin{aligned} U_z + U_t / \beta &= 0 \\ V_z + V_t / \alpha &= 0 \end{aligned} \quad (1)$$

where  $U$  and  $V$  are, respectively, the horizontal and vertical particle velocity;  $\alpha$  and  $\beta$  are, respectively, P-wave and S-wave velocity. Using backward difference operators with respect to  $z$  and  $t$ , system (1) in the Madariaga-Virieux staggered-grid scheme can be written as

$$\begin{aligned} \frac{U_{i,j}^{k-1/2} - U_{i,j-1}^{k-1/2}}{\Delta z} + \frac{U_{i,j}^{k+1/2} - U_{i,j}^{k-1/2}}{\beta_{i,j} \Delta t} &= 0 \\ \frac{V_{i+1/2,j+1/2}^{k-1/2} - V_{i+1/2,j-1/2}^{k-1/2}}{\Delta z} + \frac{V_{i+1/2,j+1/2}^{k+1/2} - V_{i+1/2,j+1/2}^{k-1/2}}{\alpha_{i+1/2,j+1/2} \Delta t} &= 0 \end{aligned} \quad (2)$$

where  $(i, j)$  is the space grid index;  $k$  is the time grid index. Figure 2-b shows a snapshot of the subsurface model with an

## Combining boundary conditions

absorbing bottom boundary. The reflections (PP and PS) from the absorbing boundary are attenuated to a low level compared to the rigid boundary, but, the absorbing boundary reflections are still stronger than the diffractor reflections, which means that the artifacts may mask the true reflections inside the medium.

A nonreflecting boundary condition (Cerjan, Kosloff, Kosloff, and Reshef, 1985) employs a strip of nodes on the boundary to attenuate wave amplitudes. These strips are also termed “numerical sponges”. For a strip width of  $N$  nodes, the amplitude values are multiplied by a factor

$$G = e^{-[\varepsilon(N-i)]^2} \quad (3)$$

where  $\varepsilon$  is a constant;  $i$  denotes the grid distance between the node and the outside boundary. Attenuating the wave amplitude by the factors has two effects. Firstly, the wave is weakened towards to the outside boundary, which means the reflection from the outside boundary will be attenuated. The second effect is that, when wave enters the energy absorbing strip, it “sees” the change in impedance of the medium and then part of the wave energy will be reflected back. Thus, for a strip width of  $N$ , there seems to exist  $N$  fictitious reflectors. Hence, there are two kinds of reflections generated from the nonreflecting boundary. One is from the fictitious reflectors; the other one is from the outside rigid boundary. The constant  $\varepsilon$  affects both reflections. The greater the constant  $\varepsilon$  is, the stronger the fictitious reflector reflections will be, but the weaker the outside rigid boundary reflection will be. The width  $N$  has little influence on the fictitious reflector reflections, while large  $N$  certainly results in weaker outside boundary reflection. Figure 2-c shows a snapshot of a nonreflecting bottom boundary, where  $N = 50$ , and  $\varepsilon = 0.004$ . The reflections from the fictitious reflectors are comparable to the point diffractor reflection, while the reflection from the outside boundary is much stronger. (We could choose a smaller  $\varepsilon$  and a greater  $N$  to reduce both reflections to the least extent, but we choose these parameters so that we can compare the result to our combined method.)

By combining absorbing boundary conditions at the outside boundary of the nonreflecting boundary strip (Figure 3), with the same strip width  $N$  for the non-reflecting boundary, the boundary reflection can be further reduced. Figure 2-d shows a snapshot of the combined boundary, where  $N = 50$ , and  $\varepsilon = 0.004$  for the nonreflecting strip. Compared to Figure 2-c, the reflection from the bottom boundary is more attenuated. (The same as mentioned with non-reflecting boundary, we choose these parameters for the sake of algorithm demonstration. We could choose smaller  $\varepsilon$  and greater  $N$  to reduce the resident reflections to the least extent.)

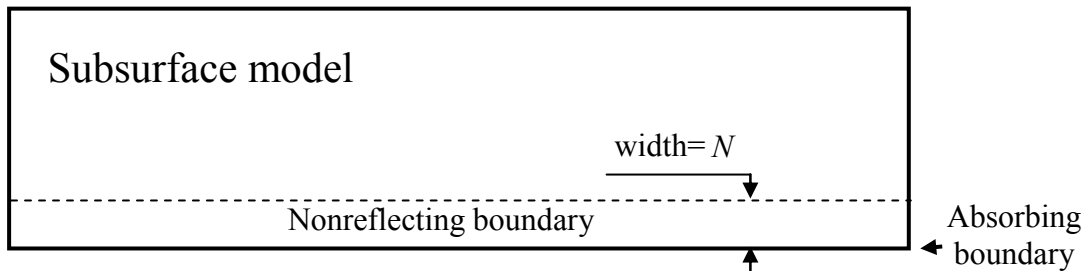


Figure 3: Combining a nonreflecting and an absorbing boundary condition at the bottom of the subsurface model.

## Conclusions

The conventional absorbing boundary conditions reduce computational edge artifacts to a low level, but these artifacts may still mask weak reflections.

The nonreflecting boundary condition produces two parts of reflections: one is from the attenuation strip which works like fictitious reflectors; the other one is from the outside boundary. To reduce both reflections, the nonreflecting strip needs to be wide, and this leads to more computational cost.

The combination the absorbing boundary conditions with the nonreflecting boundary condition results in fewer boundary artifacts with little additional computational cost.

## **Combining boundary conditions**

### **Acknowledgments**

The authors gratefully acknowledge the support of CREWES sponsor companies and various CREWES staff and students.